Time-Reversal Tunneling Effects for Cloud Radio Access Network

Hang Ma, *Student Member, IEEE,* Beibei Wang, *Senior Member, IEEE,* Yan Chen, *Senior Member, IEEE,* and K. J. Ray Liu, *Fellow, IEEE*

Abstract

The explosion of today's wireless traffic requires operators to deploy more access points (APs) and design efficient collaboration mechanism to alleviate the interference among them. However, the collaborative techniques cannot work efficiently due to the high latency and low bandwidth interface between the APs in traditional networks. To address this challenge, cloud radio access network (C-RAN) is proposed, where a pool of base band units (BBUs) are connected to the distributed remote radio heads (RRHs) via high bandwidth and low latency links (i.e., the front-haul) and are responsible for all the baseband processing. But the limited front-haul link capacity may prevent the C-RAN from fully utilizing the benefits made possible by the centralized baseband processing. As a result, the front-haul link capacity becomes a bottleneck. To address this challenge, in this work, we propose to use the time-reversal (TR) based communication as the air interface in C-RAN. Due to the unique spatial and temporal focusing effects of TR-based communications, multiple terminal devices (TDs) are naturally separated by their location-specific signatures. Such a property allows signals to be combined to deliver without demanding more bandwidth. Therefore, the TR-based communication in essence creates a "tunneling" effect such that the baseband signals for all the TDs can be efficiently combined and transmitted in the front-haul. We study the performance of the proposed C-RAN architecture in terms of spectral efficiency and front-haul rate, based on extensive measurements of the wireless channel in a real-world environment. It is shown that with nearly the same amount of traffic load in the front-haul, more information can be transmitted when there are more TDs. The proposed TR tunneling effect can help deliver more information in the C-RAN and alleviate the burden of the front-haul caused by network densification.

H. Ma is with the Department of Electrical and Computer Engineering, University of Maryland, College Park, MD, 20742 USA. He was with Origin Wireless Inc., College Park, MD 20742 USA. e-mail: hangma@umd.edu.

B. Wang and K. J. Ray Liu are with the Department of Electrical and Computer Engineering, University of Maryland, College Park, MD, 20742 USA, and with Origin Wireless Inc., College Park, MD 20742 USA. e-mail: {bebewang,kjrliu}@umd.edu.

Y. Chen was with the Department of Electrical and Computer Engineering, University of Maryland, College Park, MD, 20742 USA, and with Origin Wireless Inc., College Park, MD 20742 USA. He is now with School of Electronic Engineering, University of Electronic Science and Technology of China, Chengdu, Sichuan, China e-mail: chenyanumd@gmail.com.

With the proliferation of new mobile devices and applications, the demand for ubiquitous wireless services has increased dramatically in recent years. It has been projected that by the year 2020, the volume of the wireless traffic will rise to about 1000 times that of the year 2010 [1]. This explosion of wireless traffic will be a new challenge to wireless networks. On one hand, the huge number of wireless devices and the ever-growing data rate driven by a broad range of mobile applications lead to an unprecedented demand for network throughput, which may cause a huge deficit of spectrum. On the other hand, with a large number of coexisting wireless devices competing for network service, the scheduling delay will significantly deteriorate the user experience in many delay-sensitive applications, due to the much smaller chance of being scheduled in either coordinated networks or random access networks. In fact, people have started to feel the impact in some places, such as at the airport, conference and stadiums where it is difficult to access the wireless network with hundreds of other devices around.

To accommodate the massive devices, heterogeneous and small cell networks (HetSNets) have been considered as a promising solution. HetSNets are expected to boost data capacity through coverage expansion and load balancing. Nevertheless, with an increasing number of small cells or access points (APs) deployed, interference problems become more severe and it is necessary for multiple APs to collaborate closely in order to mitigate the interference. However, efficient collaborative radio techniques cannot work efficiently due to the high latency and low bandwidth interface between the APs in traditional wireless networks.

To address the aforementioned challenge, cloud based radio access network (C-RAN) has been proposed as a viable solution recently [2], [3], [4], [5]. It is a novel type of RAN architecture, where a pool of base band units (BBUs) are connected to the distributed remote radio heads (RRHs) via high bandwidth and low latency links. The BBUs are responsible for all the baseband processing through high performance computing. In this centralized structure, many coordinated communication schemes become possible or more efficient. For example, the coordinated multiple-point process (CoMP) in the LTE-A standard [6] can be implemented in the C-RAN to improve network capacity and energy efficiency [7]. In addition, by moving the baseband processing to the cloud, the RRHs need only support the basic transmission/reception functionalities, which further reduces their energy consumption and deployment cost.

Nevertheless, the limited front-haul link capacity [8] between the BBU and the RRH may prevent the C-RAN from fully utilizing the benefits made possible by concentrating the processing intelligence. In most of the current C-RAN structures, the data transmitted in the front-

haul is proportional to the aggregate traffic of all the terminal devices (TDs) [9], [10]. As a result, the front-haul link capacity becomes a bottleneck when there are massive TDs in the network. To tackle this challenge, several solutions have been proposed. One of them is to use compression where the baseband signal is compressed before the front-haul transmission and then de-compressed after the front-haul transmission [11], [12], [13]. Although signal compression can alleviate the traffic in the front-haul under certain cases, it introduces extra computation complexity at the RRH side, which makes this approach less cost effective. Moreover, although the compression reduces the data rate consumption of each individual TD, since the total data rate consumption is the aggregate of all the TDs, there is still a deficit of the front-haul link capacity in a dense network. An alternative solution is the sparse beamforming [9], [14], [10] where each TD is associated with a cluster of APs. However, the data rate in the front-haul link is related to the cluster size, and a larger cluster requires a higher front-haul link capacity [9]. As a result, the limited front-haul link capacity makes it impossible to fully take advantage of the available spatial diversity, which is one of the main benefits of the C-RAN structure.

Time-reversal (TR) wireless communication has been known for some time [15], [16], [17]; however, its applications have been mainly considered as a specialty use for extreme multi-path environment where other wireless communication techniques do not work well. Recently, more features of TR based wireless communication had been discovered. In [18], it is illustrated that TR based wireless communication is a "green" broadband wireless communication technique that can provide energy-efficient transmissions in the multipath-rich environments such as indoor and urban areas. Due to the unique spatial and temporal focusing effects of TR based communications, all the TDs are naturally separated by the location-specific signatures in both downlink [19] and uplink [20]. As a result, the TR-based communication becomes an efficient scheme in terms of good spatial multiplexing and much lower implementation complexity to utilize larger bandwidth, by which the achievable data rate of TR communications can outperform other wireless communication technologies, for example LTE [21]. These facts make TR a promising candidate in the future broadband wireless communication solutions, which has been illustrated in various applications, for example cognitive radio networks [22] and the internet of things (IoT) [23].

Since all the TDs are naturally separated by their signatures, the baseband signals for all the TDs can be efficiently combined and transmitted if TR communication is used as the air interface. We aim to leverage this unique feature of the TR based communications to create in essence a

tunneling effect between the BBU and RRH to alleviate the traffic load in the front-haul link of C-RAN. Specifically, in this work, we propose a C-RAN framework using TR communication as the air interface. The architectures for both downlink and uplink data transmissions are designed. We analyze the performance of both the downlink and uplink transmissions in terms of the spectral efficiency and the data rate consumption in the front-haul link. To illustrate the effectiveness of the proposed system, we conduct experiments to measure the multi-path channel information in the real-world environment, based on which we show that the TR based C-RAN creates a unique "tunneling effect" such that more information can be transmitted in the front-haul link with the same amount of bits/energy when there are more TDs in the system. This feature is highly desirable in the C-RAN system since it significantly alleviates the traffic load in the front-haul link caused by the network densification, which makes the proposed TR based C-RAN a perfect candidate to work in the multipath-rich environments such as indoor and urban areas to provide wireless connections to massive TDs using relatively broad bandwidth.

The rest of this paper is organized as follows: in section II, the system model and the working phases are introduced. We analyze the performance of the downlink and uplink schemes in section III and IV, respectively. In section V, the real-world channel measurement setting is introduced, followed by numerical results demonstrating the effectiveness of the downlink and uplink schemes. Section VI concludes the paper.

II. System Model

In this work, we consider a C-RAN in the indoor environments to accommodate the massive terminal devices (TDs) in both uplink and downlink data transmissions. The proposed system consists of multiple RRHs that connect to the cloud via front-haul links. As shown in Fig. 1, multiple RRHs are distributed in an area and transmit/receive data to/from various TDs in this area. Each of the RRHs uses TR-based communication to communicate with the TDs. All the RRHs work in the same spectrum.

In the following, we first briefly introduce the basic TR based wireless communication and then the channel model adopted in this paper. After that, we will describe the three working phases of the system in detail: the channel probing phase, the downlink data transmission phase and the uplink data transmission phase.

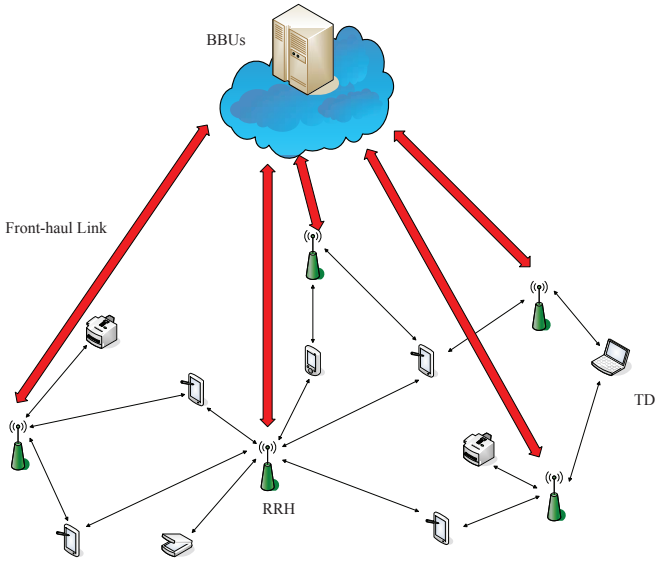

Fig. 1: The System Model

A. *Channel Model*

In the indoor broadband wireless communication, the signal suffers from the multi-path effect caused by the reflections of the indoor environment. Instead of trying to avoid the multi-path effect, TR based communication utilizes all the multi-paths to act like a matched filter to achieve spatial and temporal focusing effects. In Fig. 2, we show the typical process of a TR communication. For example, transceiver B tries to transmit some information to transceiver A. Prior to the transmission, the transceiver A has to send out a delta-like pilot pulse which propagates to transceiver B through a multi-path channel, and transceiver B keeps a record of the received waveform h. Then, the transceiver B time reverses the received waveform, and use the normalized time-reversed conjugate signals as a basic waveform g, i.e.,

$$g[k] = \frac{h^*[L-1-k]}{\sqrt{\sum_{l=0}^{L-1} \|h[l]\|^2}} \tag{1}$$

where $L = \frac{\delta_T}{T_S}$ is the channel length, T_S is the sampling period of the transceivers such that $\frac{1}{T_S}$ equals to the bandwidth B used and δ_T is the delay spread of the channel [24]. Due to the channel reciprocity, when transceiver B transmits g, the multi-path channel forms a natural matched filter by performing $h * g$, and hence a peak is expected at the receiver.

Without loss of generality, we assume that each RRH is equipped with M_T antennas and each TD is equipped with 1 antenna. We assume a multi-path Rayleigh fading channel and the

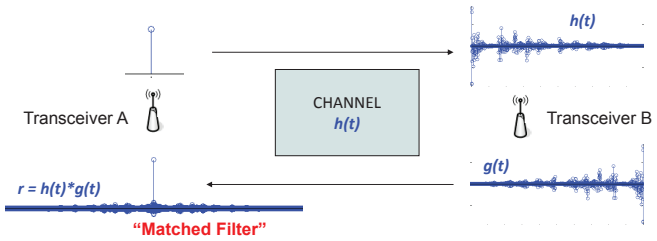

Fig. 2: The schematic diagram of the time reversal system

channel impulse response (CIR) of the communication link between the m-th antenna of the i-th RRH and the j-th TD is modeled as

$$h_{i,j}^{(m)}[k] = \sum_{l=0}^{L-1} h_{i,j}^{(m),(l)} \cdot \delta[k-l], \tag{2}$$

where $h_{i,j}^{(m),(l)}$ is the complex amplitude of the l-th tap of the CIR with length L, $h_{i,j}^{(m)}[k]$ is the k-th tap of the CIR. In practice, the $h_{i,j}^{(m)}$ is an equivalent channel which is a combination of the multi-path environment, the raised-cosine filter and the antenna. Since the raised-cosine filter and the antenna remain the same for the same radio, there is no need to counter the effects of them for TR to work. In the rest of this paper, we treat $h_{i,j}^{(m)}$ as the channel for the proposed system.

B. The TR-based C-RAN Channel Probing Phase

In the C-RAN, all the RRHs work together to serve the TDs in downlink and uplink. To achieve this, the BBUs first need to gather all the necessary information of all the TDs. In the TR-based communication, the TDs are separated naturally by their CIR's as the location-specific signature. Therefore, the BBUs need to collect the CIR information of all the TDs before all the TDs can be served. We propose the channel probing phase in the C-RAN where the BBUs get the channel information $h_{i,j}^{(m)}$'s of from all the RRHs to the TDs. In the proposed system, the system periodically switches between the channel probing, downlink transmission and uplink transmission phases. The downlink and uplink transmissions work by time division duplexing (TDD) such that the channel information can be shared by the downlink and uplink. In the following, we will first introduce the channel probing phase which is common and necessary for both downlink and uplink transmissions, after which we describe in details the downlink and uplink transmission phases respectively.

Let $\mathbf{R}$ denote the set of indices of all the RRHs, $\mathbf{T}$ the set of indices of all the TDs, $\mathbf{T}_i$ the set of indices of all the TDs subscribed to the RRH i, and $\mathbf{R}_j$ the set of the indices of all the RRHs that the j-th TD is subscribed to. Note that we have $\mathbf{T}_i \subseteq \mathbf{T}$, $\mathbf{R}_j \subseteq \mathbf{R}$.

In the channel probing phase, the N TDs first take turns to transmit a channel probing signal to all the RRHs, and the RRHs transmit the received channel probing signal through the front-haul links to the BBUs where the channel information is extracted. The channel probing signal can be an impulse signal or a pre-defined pseudo random code known by the BBUs beforehand. Since all the RRHs work in the same band, the channel probing signal transmitted by user j can be received by all the corresponding RRHs simultaneously, and the BBUs can extract the channel information between each TD and all its corresponding RRHs using various methods. For instance, the pre-defined pseudo random sequence can be the Golay sequence [25] and the channel information $h_{i,k}^{(m)}$ can be obtained by calculating the cross correlation of the transmitted Golay sequence and the sequence received by the m-th antenna of RRH i. At the end of the channel probing phase, the BBUs have the channel knowledge between all the TDs and their corresponding RRHs. Since the downlink and uplink transmissions use the TDD, the channel information works for both uplink and downlink. Moreover, since all the baseband processing is conducted in the BBUs, the TDs do not need to have the channel information in either downlink or uplink. Therefore, no feedback is needed to deliver the channel information back to the TDs.

To understand the overhead caused by the channel probing phase in the proposed system, we analyze it quantitatively. In [26], it was shown through experiments that the channel information in the indoor environment does not change in hours for a TD that does not move. On the other hand, in our experiment, we discover that the channel information changes much as one moves more than 3 cm. Therefore, frequent channel information update is needed for those TDs that are moving. For example, we consider a typical hand-held device. As the typical walking speed is 1.4 m per second, the TD needs to do channel probing every 18 ms. In the experiment described in section V of the paper, we use Golay sequence of total length 2048 as the channel probing sequence, and the sampling rate is 125 MHz. The time needed for a single channel probing is 16 μs. Compared with the channel updating period which is 18 ms, the channel probing overhead is less than 0.1% of the total time for a typical moving TD, which is comparable to the channel estimation overhead in the LTE systems [27]. While the C-RAN system has to handle the channel probing for every single TD, the system-wide overhead will be the aggregation of the individual overheads.

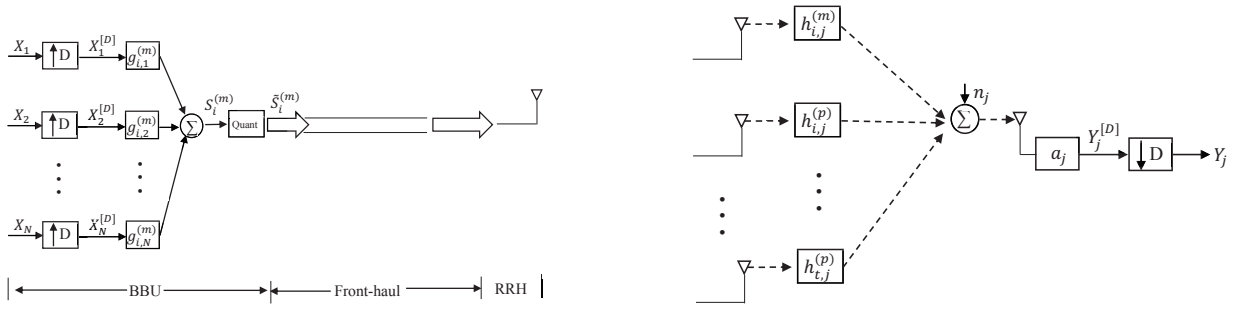

(a) BBU to RRH through Front-haul

(b) RRHs to Subscribed TD j

Fig. 3: The Two Steps in The Downlink Data Transmission Phase

An implicit feature of the proposed channel probing phase is that each TD is only subscribed to the RRHs close enough to it. The RRHs far away from the TD j can not get the channel probing signal and will not add it to the subscription list. The searching range of the TD j can be adjusted by tuning the power of the channel probing signal. Increasing the power will extend the searching range so that the TD can possibly subscribe to more RRHs. On the RRH side, this feature enables automatic power management. If an RRH is far away from all the active TDs, using this RRH to serve the TDs might not be energy efficient. In the proposed method, this RRH does not get any channel probing signal and does not use any power to transmit data to the TDs, while the TDs are better served by other RRHs closer to them.

C. The Downlink Transmission Architecture

After the channel probing phase, the BBUs start to utilize the collected channel information to serve the downlink and uplink data transmissions. The system uses TDD to support downlink and uplink transmissions. In this subsection, we describe the downlink transmission phase.

In the downlink transmission, as shown in Fig. 3, there are two steps: in step (1), the transmitted signals are calculated at the BBUs and quantized before they are transmitted through the front-haul to the RRH; in step (2), the RRH converts the baseband signals to the RF signals and transmits them to the TDs through the multi-path channel.

As shown in Fig. 3a, the intended symbol sequence $X_j[k]$ for the j-th TD transmitted from the m-th antenna of the i-th RRH is first up-sampled by the back-off factor D in order to alleviate the inter-symbol interference (ISI) and then convolved with the signature $g_{i,j}^{(m)}[k]$ of the channel

$h_{i,j}^{(m)}[k]$, which is

$$g_{i,j}^{(m)}[k] = \frac{h_{i,j}^{(m)*}[L-1-k]}{\sqrt{\sum_{t\in\mathbf{T}_i}\sum_{m=1}^{M_T}\sum_{l=0}^{L-1}|h_{i,j}^{(m)}[l]|^2}}, \quad k = 0, 1, \cdots, L-1. \tag{3}$$

where $h_{i,j}^{(m)*}[L-1-k]$ denotes the conjugate of $h_{i,j}^{(m)}[L-1-k]$.

After that, the intended signals for all the subscribed TDs at the m-th antenna of RRH i are combined as

$$S_i^{(m)}[k] = \sum_{j\in\mathbf{T}_i}\left(X_j^{[D]} * g_{i,j}^{(m)}\right)[k]. \tag{4}$$

where $\left(X_j^{[D]} * g_{i,j}^{(m)}\right)[k]$ denotes the convolution of $X_j^{[D]}[k]$ and $g_{i,j}^{(m)}[k]$.

The average power of the baseband signal $S_i^{(m)}[k]$ can be calculated as

$$E[\|S_i^{(m)}[k]\|^2] = \frac{\theta}{D} \tag{5}$$

where $\theta = E[\|X_j[k]\|^2]$.

Then the $S_i^{(m)}$ is quantized and the BBUs transmit the quantized $\tilde{S}_i^{(m)}[k]$ through the front-haul with a limited capacity. The quantization of $S_i^{(m)}$ can be modeled as

$$\tilde{S}_i^{(m)}[k] = S_i^{(m)}[k] + q_i^{(m)}[k], \tag{6}$$

where $q_i^{(m)}[k]$ is the quantization noise at the m-th antenna of RRH i. By (4), $S_i^{(m)}[k]$ is a summation of multiple independent variables and can be approximated as a complex Gaussian random variable by the law of large numbers, and $q_i^{(m)}[k]$ can be approximated as a complex random variable whose real and imaginary parts are uniformly distributed in the range $(-\frac{Q_i^{(m)}}{2}, \frac{Q_i^{(m)}}{2})$ where $Q_i^{(m)} = \frac{2K_i^{(m)}}{2^{B_i^{(m)}}}$ is the quantization level [28] of the baseband signal at the m-th antenna of i-th AP, $B_i^{(m)}$ is the number of bits used to represent the real/imaginary part of $S_i^{(m)}[k]$, and $[-K_i^{(m)}, K_i^{(m)}]$ is the dynamic range of the real/imaginary part of $S_i^{(m)}[k]$.

In step (2), each RRH i simultaneously transmits the baseband signal $\tilde{S}_i^{(m)}[k]$ via the m-th antenna over the air to all the subscribed TDs for $m = 1, 2, \cdots, M_T$, and each subscribed TD will receive the signal from all the corresponding RRHs simultaneously. The received signal is a combination of the intended signal and the interference contaminated by noise. The TD j then first amplifies the received signal with a_j and then down-samples it with the factor D, obtaining the received sequence Y_j. The noise is assumed to be zero-mean additive white gaussian noise with variance $E[|n_j[k]|^2] = \sigma^2,\ \forall j, k$. In the next section, we will investigate the received signal Y_j to analyze the performance of the proposed system in the downlink phase.

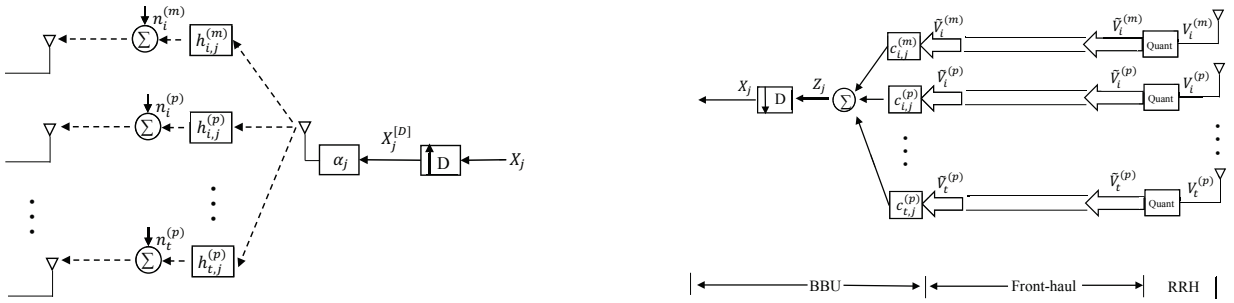

(a) TD j to All Corresponding RRHs

(b) RRHs to BBUs through front-haul link

Fig. 4: The Two Steps in The Uplink Data Transmission Phase

D. The Uplink Transmission Architecture

In the uplink transmission, as shown in Fig. 4, there are two similar steps in the opposite direction: in step (1), the TDs simultaneously transmit the data through the multi-path channels to the corresponding RRHs; in step (2), the RRHs convert the RF signal into baseband signal, and quantize them before they are transmitted via the front-haul to the BBUs. The BBUs jointly process the received baseband signal to extract the uplink data.

In step 1, all the TDs simultaneously transmit the symbol sequences over the air to the corresponding RRHs. The intended symbol sequence $X_j[k]$ from the j-th TD is first up-sampled by the back-off factor D in order to alleviate the ISI and then scaled by the factor α_j before transmitted through the multi-path channel to all the corresponding RRHs. The purpose of the scaling factor α_j is to realize the power control. It is assumed that the values of α_j's are calculated by the BBUs and signaled to the TDs through the feedback/control channel. The signal received at the m-th antenna of RRH i is a combination of the signals from all the TDs that can reach RRH i and contaminated by the white Gaussian noise upon receiving,

$$V_i^{(m)}[k] = \sum_{j \in \mathbf{T}_i} \alpha_j \left(X_j^{[D]} * h_{i,j}^{(m)} \right)[k] + n_i^{(m)}[k] \tag{7}$$

where $n_i^{(m)}[k]$ is the AWGN with variance $E[|n_i^{(m)}[k]|^2] = \sigma^2, \ \forall i, k$.

The average power of the baseband signal $V_i^{(m)}[k]$ can be calculated as

$$E[\|V_i^{(m)}[k]\|^2] = \frac{\theta \cdot \sum_{j \in \mathbf{T}_i} \alpha_j^2 \sum_{l=0}^{L-1} \|h_{i,j}^{(m)}[l]\|^2}{D} + \sigma^2 \tag{8}$$

The signal received at the RRH is then quantized and transmitted to the BBU pool through the front-haul, which can be represented as

$$\tilde{V}_i^{(m)}[k] = V_i^{(m)}[k] + q_i^{(m)}[k] \tag{9}$$

where $q_i^{(m)}[k]$ is the quantization noise. Similar to the downlink case, $q_i^{(m)}[k]$ can be approximated as a complex random variable whose real and imaginary parts are uniformly distributed in the range $(-\frac{Q_i^{(m)}}{2}, \frac{Q_i^{(m)}}{2})$. Note that although we use the same notation for the downlink and uplink quantization noise, they can be different due to distinction in the signal dynamic range and number of bits used.

Upon receiving the transmitted baseband signals from all the RRHs, the BBUs work together to extract the data of each TD. As shown in Fig. 4b, the data of TD j is extracted by combining the baseband signals from all the antennas of all the corresponding RRHs. The signal from m-th antenna of the i-th RRH is first convolved with $c_{i,j}^{(m)}$ where

$$c_{i,j}^{(m)}[k] = \frac{h_{i,j}^{(m)*}[L-1-k]}{\sqrt{\sum_{l=0}^{L-1} \|h_{i,j}^{(m)*}[l]\|^2}}, \quad k = 0, 1, \cdots, L-1. \tag{10}$$

After that, the processed signal from all the antennas of all the corresponding RRHs are combined as

$$Z_j[k] = \sum_{i \in R_j} \sum_{m=1}^{M_T} c_{i,j}^{(m)} * \tilde{V}_i^{(m)}[k]. \tag{11}$$

In section IV, we will look into the signal $Z_j[k]$ to investigate the uplink performance of the proposed system.

III. Downlink Performance Analysis

In this section, we analyze the performance of the proposed system from two perspectives, the spectral efficiency and the data rate in the front-haul. The spectral efficiency indicates how efficiently the proposed system uses the available spectrum, and the data rate in the front-haul evaluates how much capacity is necessary to deploy the proposed system.

A. Spectral Efficiency

Since all the RRHs and TDs work in the same spectrum, the signal received by each TD is a mixture of the intended signal, interference and noise. The signal received by TD j can be represented as

$$\begin{aligned} Y_j[k] &= a_j \sum_{i\in\mathbf{R}_j}\sum_{m=1}^{M_T} \tilde{S}_i^{(m)} * h_{i,j}^{(m)}[k] + a_j n_j[k] \\ &= a_j \sum_{i\in\mathbf{R}_j}\sum_{m=1}^{M_T}\sum_{t\in\mathbf{T}_i} X_t^{[D]} * g_{i,t}^{(m)} * h_{i,j}^{(m)}[k] \\ &\quad + a_j \sum_{i\in\mathbf{R}_j}\sum_{m=1}^{M_T} q_i^{(m)} * h_{i,j}^{(m)}[k] + a_j n_j[k], \end{aligned} \tag{12}$$

where, in the last equality, the first term is the intended signal combined with the interference, the second term is the received quantization noise, and the third term is the white Gaussian noise. In the following, we will analyze the first and second term subsequently.

The first term can be further written as

$$\begin{aligned} & a_j \sum_{i\in\mathbf{R}_j}\sum_{m=1}^{M_T}\sum_{t\in\mathbf{T}_i} X_t^{[D]} * g_{i,t}^{(m)} * h_{i,j}^{(m)}[k] \\ &= a_j \sum_{i\in\mathbf{R}_j}\sum_{m=1}^{M_T} X_j^{[D]} * g_{i,j}^{(m)} * h_{i,j}^{(m)}[k] \\ &\quad + \sum_{i\in\mathbf{R}_j}\sum_{m=1}^{M_T}\sum_{\substack{l=0 \\ l\neq\frac{L-1}{D}}}^{\frac{2L-2}{D}} X_j[k+\frac{L-1}{D}-l]\cdot g_{i,j}^{(m)} * h_{i,j}^{(m)}[Dl] \\ &\quad + \sum_{i\in\mathbf{R}_j}\sum_{m=1}^{M_T}\sum_{\substack{t\in\mathbf{T}_i \\ t\neq j}}\sum_{l=0}^{\frac{2L-2}{D}} X_t[k+\frac{L-1}{D}-l] * g_{i,t}^{(m)} * h_{i,j}^{(m)}[Dl]. \end{aligned} \tag{13}$$

The first term is the intended signal for TD j, the second term is the ISI, and the third term is the inter-user interference (IUI). Note that by the channel reciprocity in the channel probing phase, for any RRH u with $u \notin \mathbf{R}_j$, TD j and RRH u can not reach each other and therefore TD j does not suffer from the interference from RRH u.

Since the one-tap gain a_j does not affect the SINR, we assume it as $a_j = 1$ in the subsequent analysis, without loss of generality.

The signal power in the downlink can be written as

$$P_{sig}^{(dl)} = E_X[\| \sum_{i\in\mathbf{R}_j} \sum_{m=1}^{M_T} X_j[k] \cdot g_{i,j}^{(m)} * h_{i,j}^{(m)}[L-1]\|^2]$$
$$= \theta \| \sum_{i\in\mathbf{R}_j} \sum_{m=1}^{M_T} g_{i,j}^{(m)} * h_{i,j}^{(m)}[L-1]\|^2. \tag{14}$$

Accordingly, the ISI and IUI power can be written as

$$P_{isi}^{(dl)}$$
$$= E_X[\| \sum_{i\in\mathbf{R}_j} \sum_{m=1}^{M_T} \sum_{\substack{l=0 \\ l\neq\frac{L-1}{D}}}^{\frac{2L-2}{D}} X_j[k+\frac{L-1}{D}-l] \cdot g_{i,j}^{(m)} * h_{i,j}^{(m)}[Dl]\|^2]$$
$$= \theta \sum_{\substack{l=0 \\ l\neq\frac{L-1}{D}}}^{\frac{2L-2}{D}} \| \sum_{i\in\mathbf{R}_j} \sum_{m=1}^{M_T} g_{i,j}^{(m)} * h_{i,j}^{(m)}[Dl]\|^2, \tag{15}$$

and

$$P_{iui}^{(dl)}$$
$$= E_X[\| \sum_{i\in\mathbf{R}_j} \sum_{m=1}^{M_T} \sum_{\substack{t\in\mathbf{T}_i \\ t\neq j}} \sum_{l=0}^{\frac{2L-2}{D}} X_t[k+\frac{L-1}{D}-l] * g_{i,t}^{(m)} * h_{i,j}^{(m)}[Dl]\|^2]$$
$$= \theta \sum_{l=0}^{\frac{2L-2}{D}} \| \sum_{i\in\mathbf{R}_j} \sum_{m=1}^{M_T} \sum_{\substack{t\in\mathbf{T}_i \\ t\neq j}} g_{i,t}^{(m)} * h_{i,j}^{(m)}[Dl]\|^2. \tag{16}$$

Next, we analyze the quantization noise in the received signal. From (12), we can have the quantization noise power as

$$\sigma_{q,(dl)}^2 = E[\| \sum_{i\in\mathbf{R}_j} \sum_{m=1}^{M_T} q_i^{(m)} * h_{i,j}^{(m)}[k]\|^2]$$
$$= E[\sum_{i\in\mathbf{R}_j} \sum_{m=1}^{M_T} \| \sum_{l=0}^{L-1} h_{i,j}^{(m)}[l] \cdot q_i^{(m)}[k-l]\|^2]$$
$$= \sum_{i\in\mathbf{R}_j} \sum_{m=1}^{M_T} \sum_{l=0}^{L-1} \|h_{i,j}^{(m)}[l]\|^2 \cdot E[\|q_i^{(m)}[k]\|^2], \tag{17}$$

since we assume that $q_i^{(m)}$ is independent of $h_{i,j}^{(m)}$. By [28], we have

$$E[\|q_i^{(m)}[k]\|^2] = \frac{(Q_i^{(m)})^2}{12} + \frac{(Q_i^{(m)})^2}{12} = \frac{(Q_i^{(m)})^2}{6} \tag{18}$$

which is the summation of the quantization noise power in the real and imaginary parts.

The spectral efficiency of the TD j can be defined as

$$r_j^{(dl)} = \log_2(1 + \frac{P_{sig}^{(dl)}}{P_{isi}^{(dl)} + P_{iui}^{(dl)} + \sigma_{q,(dl)}^2 + \sigma^2})/D \tag{19}$$

B. Front-haul Rate

In this subsection, we analyze the front-haul rate in the proposed system in the downlink mode. As shown in Fig. 3a, in the downlink mode, the quantized signal $\tilde{S}_i^{(m)}[k]$ is transmitted from the BBUs to the RRH through the front-haul. The data rate in the front-haul connecting the BBUs and the i-th RRH can be expressed as

$$R_{fh,i} = 2 \cdot W \cdot \sum_{m=1}^{M_T} B_i^{(m)} \tag{20}$$

where W is the bandwidth of the system. It can be seen that $R_{fh,i}$ is solely dependent on the number of bits used for each symbol given the bandwidth of the system and the number of transmitting antennas. If $B_i^{(m)}$ is large, the power of the quantization noise goes down while the data rate in the front-haul increases, and vice versa if $B_i^{(m)}$ is small.

By (18), if the dynamic range $K_i^{(m)}$ of the signal grows, it needs to increase $B_i^{(m)}$ to keep the same quantization noise level. In section V, we will show through numerical results that $K_i^{(m)}$ does not change much as the number of TDs in the system grows, and therefore the proposed system has a "tunneling" effect such that the front-haul rate keeps almost constant while serving more TDs.

IV. Uplink Performance Analysis

In this section, we analyze the uplink performance of the proposed system in two perspectives: the spectral efficiency and the data rate in the front-haul.

A. Spectral Efficiency

The combined signal can be written as

$$\begin{aligned} Z_j[k] &= \sum_{i\in\mathbf{R}_j}\sum_{m=1}^{M_T}\tilde{V}_i^{(m)} * c_{i,j}^{(m)}[k] \\ &= \sum_{i\in\mathbf{R}_j}\sum_{m=1}^{M_T}\sum_{t\in\mathbf{T}_i}\alpha_t X_t^{[D]} * h_{i,t}^{(m)} * c_{i,j}^{(m)}[k] \\ &\quad + \sum_{i\in\mathbf{R}_j}\sum_{m=1}^{M_T} q_i^{(m)} * c_{i,j}^{(m)}[k] + \sum_{i\in\mathbf{R}_j}\sum_{m=1}^{M_T} n_i^{(m)} * c_{i,j}^{(m)}[k] \end{aligned} \tag{21}$$

where the first term is the mixture of the intended signal and interference for TD j, the second term is caused by the quantization noise and the third term is caused by the white Gaussian noise. In the following, we will analyze them subsequently.

The first term can be further written as

$$\begin{aligned} &\sum_{i\in\mathbf{R}_j}\sum_{m=1}^{M_T}\sum_{t\in\mathbf{T}_i}\alpha_t X_t^{[D]} * h_{i,t}^{(m)} * c_{i,j}^{(m)}[k] \\ &= \sum_{i\in\mathbf{R}_j}\sum_{m=1}^{M_T}\alpha_j X_j^{[D]} * h_{i,j}^{(m)} * c_{i,j}^{(m)}[k] \\ &\quad + \sum_{i\in\mathbf{R}_j}\sum_{m=1}^{M_T}\sum_{\substack{l=0 \\ l\neq\frac{L-1}{D}}}^{\frac{2L-2}{D}}\alpha_j X_j[k+\frac{L-1}{D}-l]\cdot h_{i,j}^{(m)} * c_{i,j}^{(m)}[Dl] \\ &\quad + \sum_{i\in\mathbf{R}_j}\sum_{m=1}^{M_T}\sum_{\substack{t\in\mathbf{T}_i \\ t\neq j}}\sum_{l=0}^{\frac{2L-2}{D}}\alpha_t X_t[k+\frac{L-1}{D}-l] * h_{i,t}^{(m)} * c_{i,j}^{(m)}[Dl]. \end{aligned} \tag{22}$$

The first term in (22) is the intended signal from TD j, the second term is the ISI, and the third term is the IUI.

The signal power in the uplink can be written as

$$\begin{aligned} P_{sig}^{(ul)} &= E_X[\|\sum_{i\in\mathbf{R}_j}\sum_{m=1}^{M_T}\alpha_j X_j[k]\cdot h_{i,j}^{(m)} * c_{i,j}^{(m)}[L-1]\|^2] \\ &= |\alpha_j|^2\theta\|\sum_{i\in\mathbf{R}_j}\sum_{m=1}^{M_T} h_{i,j}^{(m)} * c_{i,j}^{(m)}[L-1]\|^2, \end{aligned} \tag{23}$$

where $\theta = E[\|X_j[k]\|^2]$. Accordingly, the ISI and IUI power can be written as

$$P_{isi}^{(ul)} =$$

$$E_X[\| \sum_{i\in\mathbf{R}_j} \sum_{m=1}^{M_T} \sum_{\substack{l=0 \\ l\neq\frac{L-1}{D}}}^{\frac{2L-2}{D}} \alpha_j X_j[k+\frac{L-1}{D}-l]\cdot h_{i,j}^{(m)} * c_{i,j}^{(m)}[Dl]\|^2]$$

$$= |\alpha_j|^2\theta \sum_{\substack{l=0 \\ l\neq\frac{L-1}{D}}}^{\frac{2L-2}{D}} \| \sum_{i\in\mathbf{R}_j} \sum_{m=1}^{M_T} h_{i,j}^{(m)} * c_{i,j}^{(m)}[Dl]\|^2, \tag{24}$$

and

$$P_{iui}^{(ul)} =$$

$$E_X[\| \sum_{i\in\mathbf{R}_j} \sum_{m=1}^{M_T} \sum_{\substack{t\in\mathbf{T}_i \\ t\neq j}} \sum_{l=0}^{\frac{2L-2}{D}} \alpha_t X_t[k+\frac{L-1}{D}-l] * h_{i,t}^{(m)} * c_{i,j}^{(m)}[Dl]\|^2]$$

$$= \theta \sum_{l=0}^{\frac{2L-2}{D}} \| \sum_{i\in\mathbf{R}_j} \sum_{m=1}^{M_T} \sum_{\substack{t\in\mathbf{T}_i \\ t\neq j}} \alpha_t \cdot h_{i,t}^{(m)} * c_{i,j}^{(m)}[Dl]\|^2. \tag{25}$$

In this work, we assume the α_j is chosen as

$$\alpha_j = \frac{\eta}{\sum_{i\in\mathbf{R}_j} \sum_{m=1}^{M_T} h_{i,j}^{(m)} * c_{i,j}^{(m)}[L-1]} \tag{26}$$

where η is a scalar common for all the TDs. In this way, $\alpha_j \cdot \sum_{i\in\mathbf{R}_j} \sum_{m=1}^{M_T} h_{i,j}^{(m)} * c_{i,j}^{(m)}[L-1]$ is common for all the TDs, which ensures that the signal power for all the TDs are the same according to (23). The parameter η can be adjusted according to the maximum transmitting power allowed at each TD.

Next, we analyze the quantization noise in the received signal. From (21), we can have the quantization noise power as

$$\begin{aligned}\sigma_{q,(ul)}^2 &= E[\| \sum_{i\in\mathbf{R}_j} \sum_{m=1}^{M_T} q_i^{(m)} * c_{i,j}^{(m)}[k]\|^2] \\ &= E[\sum_{i\in\mathbf{R}_j} \sum_{m=1}^{M_T} \| \sum_{l=0}^{L-1} c_{i,j}^{(m)}[l]\cdot q_i^{(m)}[k-l]\|^2] \\ &= \sum_{i\in\mathbf{R}_j} \sum_{m=1}^{M_T} \sum_{l=0}^{L-1} \|c_{i,j}^{(m)}[l]\|^2 \cdot E[\|q_i^{(m)}[k]\|^2],\end{aligned} \tag{27}$$

since we can assume that $q_i^{(m)}$ is independent of $c_{i,j}^{(m)}$. Similar to the downlink scenario, we have

$$E[\|q_i^{(m)}[k]\|^2] = \frac{(Q_i^{(m)})^2}{12} + \frac{(Q_i^{(m)})^2}{12} = \frac{(Q_i^{(m)})^2}{6}. \tag{28}$$

The last term in (21) is the AWGN collected from all the corresponding antennas of TD j. Its power can be calculated by

$$\sigma_{n,(ul)}^2 = E[\| \sum_{i \in \mathbf{R}_j} \sum_{m=1}^{M_T} n_i^{(m)} * c_{i,j}^{(m)}[k]\|^2] = |\mathbf{R}_j| * M_T * \sigma^2 \tag{29}$$

where $|\mathbf{R}_j|$ stands for the cardinality of the set $\mathbf{R}_j$. We can see that the AWGN functions differently in the downlink and uplink. In the downlink, since the AWGN affects the TD when the TD receives the signal, it does not depend on the number of corresponding antennas. On the other hand, in the uplink, since the AWGN is gathered when each of the corresponding antennas receives the signal, the noise power scales up with the number of corresponding antennas.

The spectral efficiency of the TD j in the uplink can be defined as

$$r_j^{(ul)} = \log_2(1 + \frac{P_{sig}^{(ul)}}{P_{isi}^{(ul)} + P_{iui}^{(ul)} + \sigma_{q,(ul)}^2 + \sigma_{n,(ul)}^2})/D \tag{30}$$

B. Front-haul Rate

In this subsection, we analyze the front-haul rate in the proposed system in the uplink mode. As shown in Fig. 4a, in the uplink mode, the quantized signal $\tilde{V}_i[k]$ is transmitted from the RRH to the BBU through the front-haul. Similar to the downlink case, the data rate in the front-haul can be expressed as

$$R_{fh,i} = 2 \cdot W \cdot \sum_{m=1}^{M_T} B_i^{(m)}. \tag{31}$$

Similar to the downlink mode, $R_{fh,i}$ is solely dependent on the number of bits used for each symbol given the bandwidth of the system and the number of transmitting antennas. If $B_i^{(m)}$ is large, the power of the quantization noise goes down while the data rate in the front-haul increases, and vice versa if $B_i^{(m)}$ is small.

By (28), if the dynamic range $K_i^{(m)}$ of the signal grows, it needs to increase $B_i^{(m)}$ to keep the same quantization noise level. In the uplink, the total baseband signal power is dependent on the number of TDs, which is different from the downlink scenario. Therefore, when the number of TDs increases in the system, the dynamic range $K_i^{(m)}$ grows, where more bits are needed to keep the same quantization noise level.

In the next section, we will show through numerical results how $K_i^{(m)}$ and $B_i^{(m)}$ change with the number of TDs in the system.

V. Performance Evaluation

In this section, we evaluate the performance of the proposed system using measured channels. We first introduce the experimental setting where we measure the multi-path channels. Then we show some numerical results obtained by using the measured channels.

A. Channel Measurement

We build a TR radio prototype to measure the multi-path channels. A snapshot of the radio stations of our prototype is illustrated in Fig. 5, where a single antenna is attached to a small cart with RF board and computer installed on the cart. The tested signal bandwidth spans from 5.3375 GHz to 5.4625 GHz, centered at 5.4 GHz. An office room in the J. H. Kim Engineering Building at the University of Maryland is used as the measurement site. As shown in Fig. 6a, the RRHs are placed at 6 locations across the room, while the TDs are placed in multiple locations in the small room marked with "A". The layout of room "A" and an example of the placement of the TDs are shown in Fig. 6b. We measure the multi-path channels from each RRH to the TDs at all the possible locations. In this experiment, we have 800 possible TD locations and 6 possible AP locations, from which 4800 independent multi-path channel measurements are obtained. In the following subsections, the performance of the proposed system is evaluated using the measured channels.

B. Downlink Front-haul Rate and Spectral Efficiency

In this subsection, we show the unique features of the proposed system in the downlink through numerical results. We first show that the front-haul rate keeps almost constant independent of the number of TDs in the system, after which we show the achievable spectral efficiency of the system under various settings in deployment and load. We also compare the result with the C-RAN based on LTE to show the advantage of the proposed system in being able to utilize the wireless channel more efficiently.

In Fig. 7 and 8, we generate the baseband signal $S_i^{(m)}[k]$ according to (4) using the measured channels and show the complementary cumulative distribution function (CCDF) [29] of the peak to average power ratio (PAPR) of the signal $S_i^{(m)}[k]$ in-band (I) and quadrature (Q) parts under

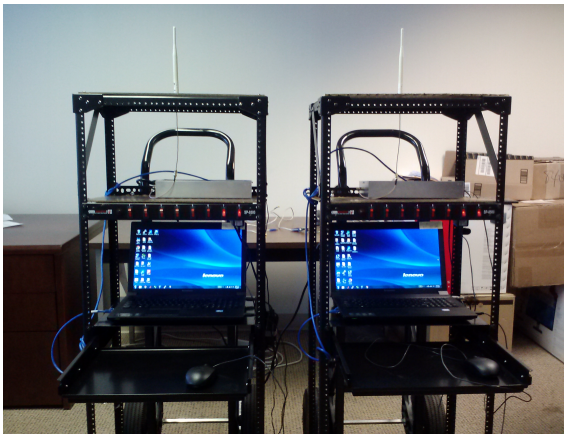

Fig. 5: The TR Radio Prototype

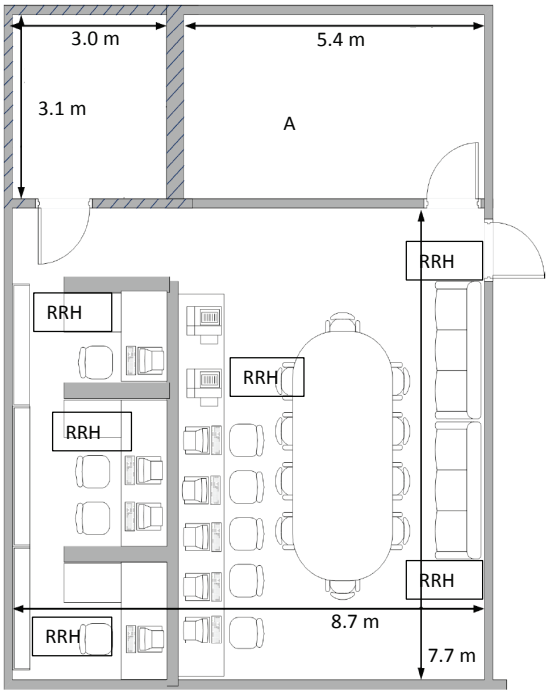

(a) The Floor Plan of The Testing Room

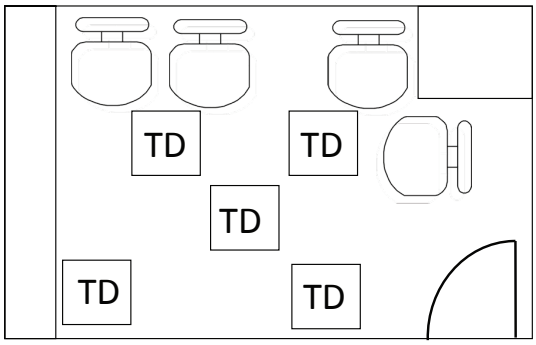

(b) Floor Plan of Room A

Fig. 6: The Floor Plan of the Testing Sites

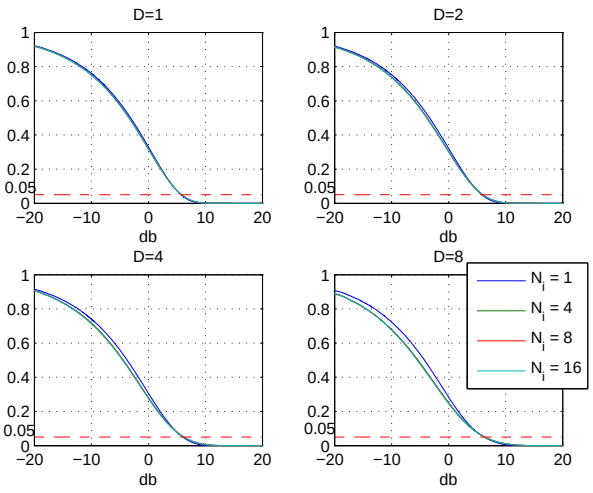

Fig. 7: The CCDF of Downlink QPSK Baseband Signal PAPR (I)

various conditions. The $X_j[k]$'s are QPSK modulated. Let $N_i = \|\mathbf{T}_i\|$ denote the number of TDs subscribed to RRH i, and it is shown that the PAPR of the $S_i^{(m)}[k]$ does not change much with N_i. For example, if we look at the dotted horizontal line at $CCDF = 0.05$, it always crosses the curves at around 6 db. The detailed statistics are shown in Table I. It means 95% of the baseband symbols $S_i^{(m)}[k]$ have the power no more than 4 times the average power. By (5), the average power of $S_i^{(m)}[k]$ is only dependent on θ and D. Therefore, the dynamic range $[-K_i^{(m)}, K_i^{(m)}]$ of $S_i^{(m)}[k]$ changes very little for different N_i's, where some $B_i^{(m)}$ can be used to always maintain the same level of quantization noise power. As a result, the data rate in each front-haul link is constant.

TABLE I: the 5% PAPR for Different N_i's in Downlink (db)

	$N_i = 1$	$N_i = 4$	$N_i = 8$	$N_i = 16$
D = 1, (I)	5.74	5.86	6.06	6.26
D = 1, (Q)	5.74	5.88	6.06	6.26
D = 2, (I)	5.86	6.02	6.22	6.36
D = 2, (Q)	5.86	6.04	6.22	6.36
D = 4, (I)	5.88	6.04	6.24	6.36
D = 4, (Q)	5.86	6.04	6.22	6.36
D = 8, (I)	5.88	6.04	6.24	6.36
D = 8, (Q)	5.88	6.04	6.22	6.36

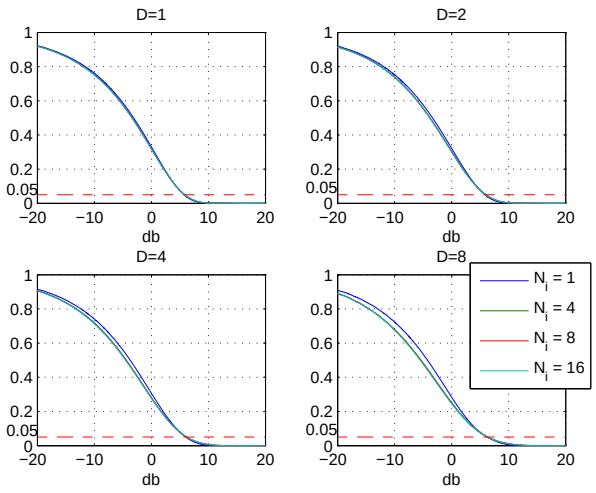

Fig. 8: The CCDF of Downlink QPSK Baseband Signal PAPR (Q)

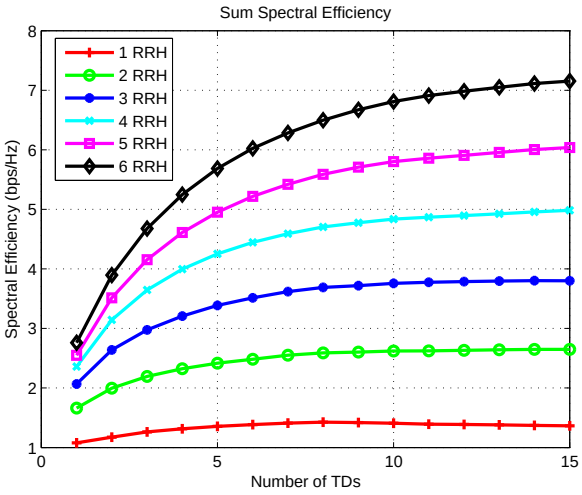

Fig. 9: The Sum Spectral Efficiency (D=1)

Next, we evaluate the spectral efficiency of the system with different number of RRHs and TDs. For each single channel realization, the $P_{sig}^{(dl)}$, $P_{isi}^{(dl)}$, $P_{iui}^{(dl)}$, and $\sigma_{q,(dl)}^2$ can be calculated by (14), (15), (16) and (17). By plugging them into (19), the spectral efficiency of each individual TD can be calculated. By averaging over all the channel realizations, we show the average and sum spectral efficiency in Fig. 9 through 12.

As shown in the figures, for each given number of RRHs in this system, the individual spectral efficiency decreases with more TDs in the system, while the sum spectral efficiency increases

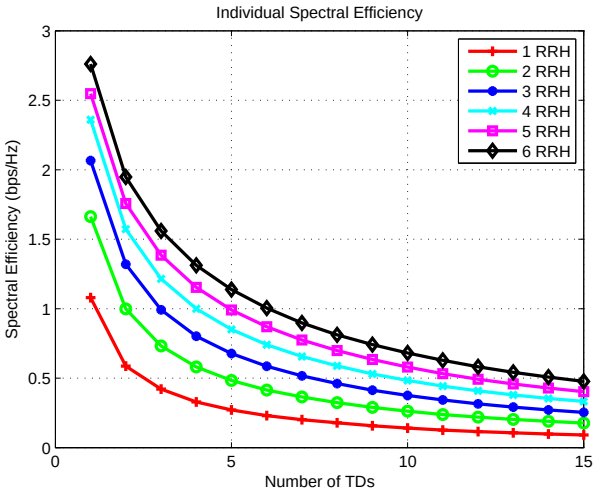

Fig. 10: The Individual Spectral Efficiency (D=1)

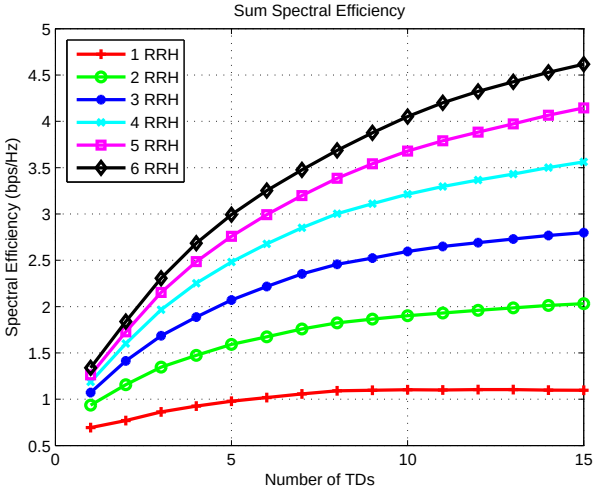

Fig. 11: The Sum Spectral Efficiency (D=4)

with more TDs in the system. Note that by previous analysis, the data rate in the front-haul keeps constant. It means that more information can be transmitted in the front-haul link with the same amount of bits and energy consumed. The reason is that by using TR-based air interface, multiple TDs are naturally separated by the location-specific signatures. Therefore, even though the baseband signals for multiple TDs are mixed together in the front-haul link, they can still be separated when transmitted through the air interface. In other words, with the TR-based air interface, we are able to create a "tunnel" in the front-haul link such that the baseband signals

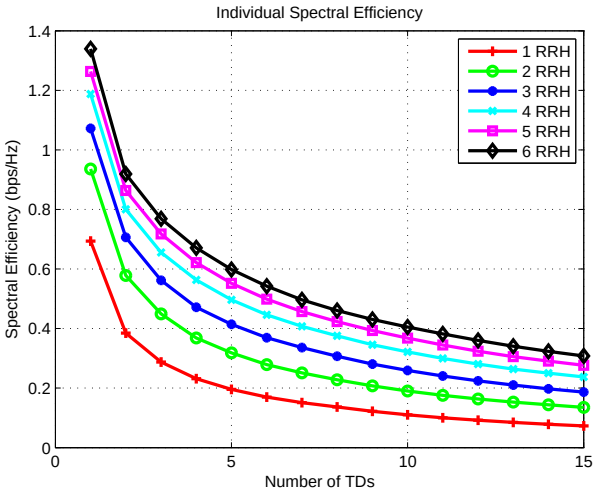

Fig. 12: The Individual Spectral Efficiency (D=4)

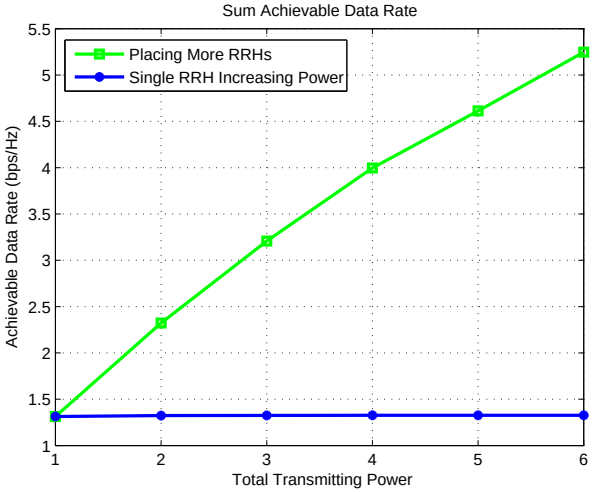

Fig. 13: The Comparison between Adding More RRHs and Single RRH Increasing Power

can be efficiently combined to alleviate the traffic in front-haul.

Moreover, it can be observed that both the individual and sum spectral efficiency are improved if more RRHs are added into this system. The new RRHs contribute both extra power and degree of freedom to the system. The extra power alleviates the influence of the quantization and environmental noise, while the extra degree of freedom helps enhancing the focusing effect [18] and thus mitigating the interference. Usually, in a dense wireless network, the interference is the dominating factor that limits the performance of the system. To illustrate this phenomenon,

we compare the effect of adding in more RRHs with that of increasing the power of a single RRH. As it can be seen from Fig. 13, the blue curve shows that by just increasing the power of one single RRH, the spectral efficiency keeps almost constant, while the green curve shows that by adding in more RRHs, the spectral efficiency is improved significantly.

C. Uplink Front-haul Rate and Spectral Efficiency

In this subsection, we show through numerical results to illustrate the effectiveness of the proposed system in the uplink.

In Fig. 14 and 15, we generate the baseband signal $V_i^{(m)}[k]$ according to (7) using the measured channels and show the CCDF of the PAPR of both I and Q parts of the signal $V_i^{(m)}[k]$ under various conditions. The $X_j[k]$'s are QPSK modulated. It is shown that the PAPR of $V_i^{(m)}[k]$ does not change much with the number of TDs subscribed to the RRH i. Similarly, the $CCDF = 0.05$ line always crosses the CCDF curves at around 6 db. The detailed statistics are shown in Table II. It means 95% of the baseband symbols $V_i^{(m)}[k]$ have the power no more than 4 times the average power. By plugging (26) into (8), the average power of $V_i^{(m)}[k]$ can be calculated as

$$E[\|V_i^{(m)}[k]\|^2] = \frac{\eta^2\theta}{D} \cdot \sum_{j\in\mathbf{T}_i} \frac{\sum_{l=0}^{L-1} \|h_{i,j}^{(m)}\|^2}{(\sum_{t\in\mathbf{R}_j} \sum_{m=1}^{M_T} h_{t,j}^{(m)} * c_{t,j}^{(m)}[L-1])^2} + \sigma^2, \tag{32}$$

which grows approximately linearly with N_i. Therefore, the dynamic range $[-K_i^{(m)}, K_i^{(m)}]$ of $V_i^{(m)}[k]$ increases linearly with $\sqrt{N_i}$. In order to maintain the same level of quantization noise power, more bits are needed to represent $V_i^{(m)}[k]$. However, since $Q_i^{(m)} = \frac{2K_i^{(m)}}{2^{B_i^{(m)}}}$, in order to maintain the same level of quantization noise power, $B_i^{(m)}$ grows to the order of $\log_2(K_i^{(m)})$ and thus $\log_2(\sqrt{N_i})$. For example, $E[\|q_i^{(m)}[k]\|^2]$ is the same for $B_i^{(m)} = 12, N_i = 1$ and $B_i^{(m)} = 14, N_i = 16$. In other words, when there are more TDs in the system, it is necessary to use slightly more bits in the front-haul link, which is much less significant compared to the increase of the number of TDs.

Similar to the downlink scenario, we evaluate the spectral efficiency of uplink by averaging over all the channel realizations. We slightly increase $B_i^{(m)}$ when it is necessary to keep the same level of quantization noise power. We show the average and sum spectral efficiencies under various conditions in Fig. 16 through Fig. 19 and observe similar trends as in downlink.

Similar to the downlink scenario, the "tunneling" effect is also observed in the uplink case. When there are more TDs in the system, with using almost the same amount of bits in the front-haul link, more information can be extracted at the BBU side.

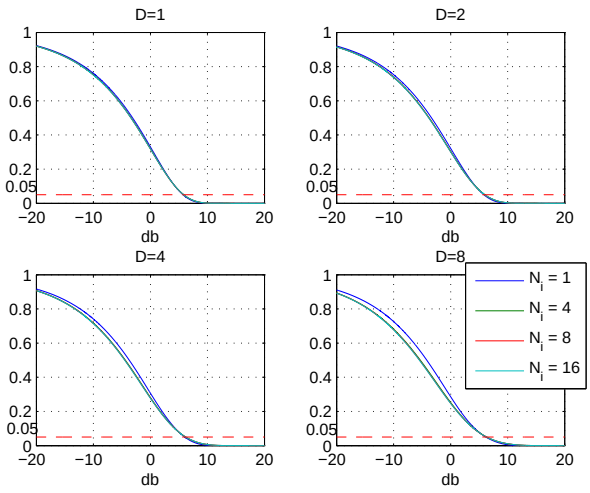

Fig. 14: The CCDF of Uplink QPSK Baseband Signal PAPR (I)

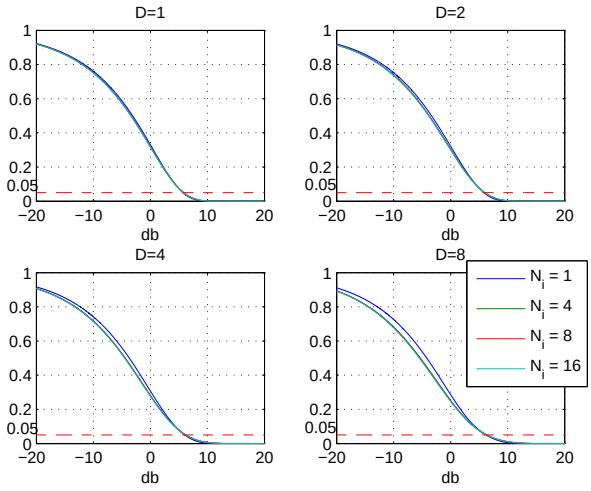

Fig. 15: The CCDF of Uplink QPSK Baseband Signal PAPR (Q)

D. Comparison with LTE based C-RAN

To illustrate the advantage of the TR "tunneling" effect in the C-RAN, in this subsection, we compare the proposed system with LTE based C-RAN in multiple scenarios.

Suppose we have a certain number of RRHs distributed in an area where there are N TDs and each of them has Ω bits of data to be transmitted. We first consider the donwlink. In the LTE based C-RAN, all the RRHs work in separate bands, and each of the RRHs is responsible for serving part of the TDs. Since each RRH serves multiple TDs by dividing the time and/or

TABLE II: the 5% PAPR for Different N_i's in Uplink (db)

	$N_i = 1$	$N_i = 4$	$N_i = 8$	$N_i = 16$
D = 1, (I)	5.74	5.86	6.06	6.22
D = 1, (Q)	5.74	5.88	6.06	6.22
D = 4, (I)	5.86	6.02	6.22	6.34
D = 4, (Q)	5.86	6.02	6.22	6.36
D = 8, (I)	5.88	6.04	6.22	6.36
D = 8, (Q)	5.86	6.04	6.22	6.36
D = 16, (I)	5.88	6.04	6.24	6.36
D = 16, (Q)	5.88	6.04	6.22	6.36

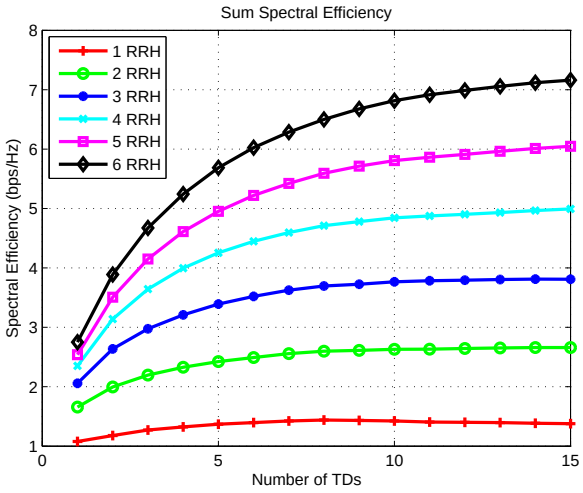

Fig. 16: The Sum Spectral Efficiency (D=1)

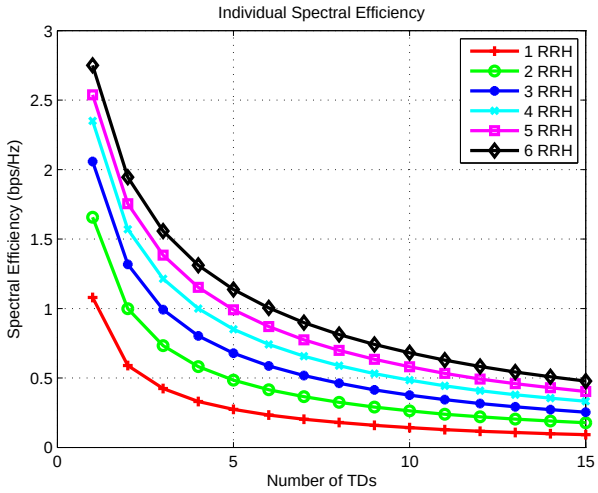

Fig. 17: The Individual Spectral Efficiency (D=1)

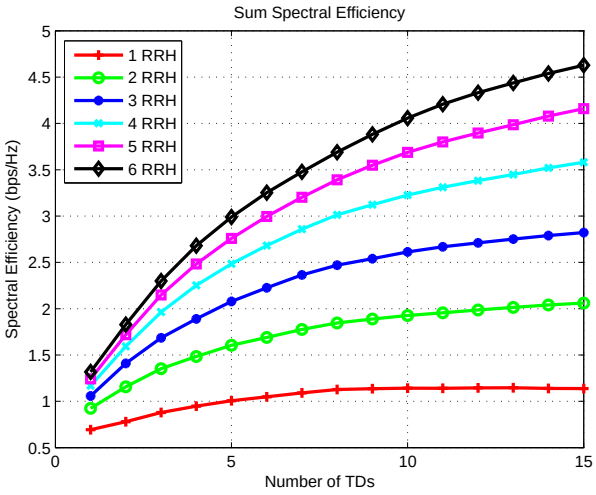

Fig. 18: The Sum Spectral Efficiency (D=4)

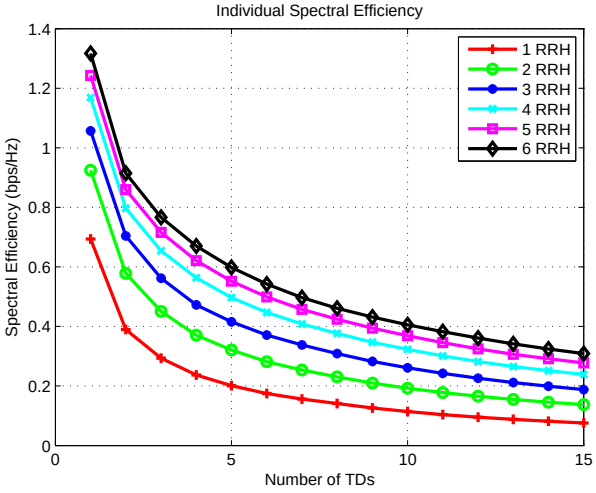

Fig. 19: The Individual Spectral Efficiency (D=4)

frequency resource, the baseband signals for multiple TDs cannot be mixed together. As a result, the total amount of baseband signal is proportional to $N \times \Omega$, which can be approximated by $\phi_N^{(dl)} = N \times \Omega \times \lambda^{(dl)}$ where $\lambda^{(dl)}$ is some constant accounting for the modulation and channel coding. On the other hand, in the TR based C-RAN, as analyzed in section V-B, the data for multiple TDs can be efficiently combined without increasing the traffic in the front-haul. As a result, the total amount of baseband signal transmitted in the front-haul link is constant independent of N, which can be approximated by $\varphi_N^{(dl)} = \Omega \times \mu^{(dl)}$ where $\mu^{(dl)}$ is some constant

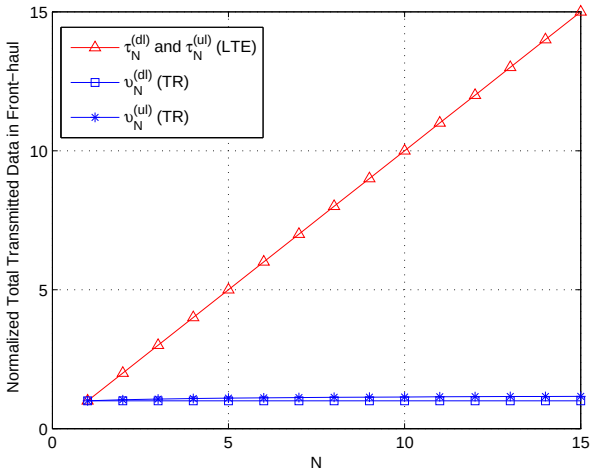

Fig. 20: The Comparison of Normalized Total Transmitted Data in Front-haul between TR based C-RAN and LTE based C-RAN

accounting for the modulation and channel coding. We define $\tau_N^{(dl)} = \frac{\phi_N^{(dl)}}{\phi_1^{(dl)}}$ and $\upsilon_N^{(dl)} = \frac{\varphi_N^{(dl)}}{\varphi_1^{(dl)}}$ to characterize the growth of data transmitted in the front-haul caused by increasing the number of TDs.

In the uplink, the LTE works by single-carrier frequency division multiple access (SC-FDMA) [30], where multiple TDs are separated by the division of the frequency resource. As a result, the aggregate data transmitted in the front-haul is also proportional to $N \times \Omega$, and $\tau_N^{(ul)}$ is the same as the $\tau_N^{(dl)}$. On the other hand, in the TR based C-RAN, as analyzed in section V-C, the data transmitted in the front-haul only increases slightly. We define $\varphi_N^{(ul)} = \Omega \times B_N^{(ul)} \times \mu^{(ul)}$ where $B_N^{(ul)}$ is the average number of bits to represent a baseband signal symbol when there are N TDs, and similarly $\upsilon_N^{(ul)} = \frac{\varphi_N^{(ul)}}{\varphi_1^{(ul)}}$. In this example, we have $B_1^{(ul)} = 12$ and $B_N^{(ul)}$ is increased when necessary according to the analysis in section IV-B.

In Fig. 20, we show the $\tau_N^{(dl)}$, $\tau_N^{(ul)}$, $\upsilon_N^{(dl)}$ and $\upsilon_N^{(ul)}$ with different N's. It is illustrated that in both downlink and uplink, the total amount of data transmitted in the front-haul of LTE based C-RAN increases linearly with the number of TDs. In contrast, the total amount of data transmitted in the front-haul of TR based C-RAN keeps constant in the downlink regardless of the number of TDs, while only slightly increases in the uplink. It is due to the unique "tunneling" effect such that more information can be transmitted with nearly the same amount of bits consumed in the front-haul.

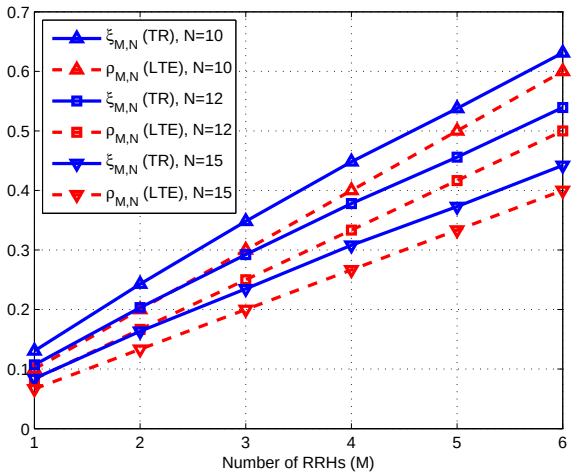

Fig. 21: The Comparison of Normalized Effective Individual Spectral Efficiency between TR based C-RAN and LTE based C-RAN

We also compare the spectral efficiency of the proposed system with that of LTE based C-RAN. Suppose there are N TDs distributed in an area to be served. We gradually add in extra RRHs to the C-RAN. In the TR based C-RAN, the extra RRHs mainly help enhance the focusing effect and thus improve the spectral efficiency. More specifically, we define $r_{M,N}^{(avg)}$ as the average spectral efficiency of an individual TD when there are M RRHs and N TDs in the system. To evaluate the effect of adding in extra RRHs and TDs, we define

$$\xi_{M,N} = \frac{r_{M,N}^{(avg)}}{r_{1,1}^{(avg)}}, \tag{33}$$

which normalizes the average spectral efficiency to that when the wireless channel is exclusively used by a single pair of RRH and TD.

On the other hand, in the LTE based C-RAN, we assume that each TD is associated with only one RRH and multiple RRHs work in separate bands. The extra RRHs will offload part of the TDs from the existing RRHs, and thus each TD has an improved chance of being scheduled. Similar to the TR-based C-RAN, we define the effective average spectral efficiency $\delta_{M,N}^{(avg)} = C_{M,N}^{(avg)} \cdot \beta_{M,N}^{(avg)}$ where $\beta_{M,N}^{(avg)}$ is the average portion of time and frequency resource that a single TD shares when there are M RRHs and N TDs, and $C_{M,N}^{(avg)}$ is the average spectral efficiency of a TD conditioning on it is scheduled and allocated the entire time and frequency resource of a RRH. Since the RRHs work in separate bands, $C_{M,N}^{(avg)}$ does not change with M or N, and $\beta_{M,N}^{(avg)} = \min(\frac{M}{N}, 1)$.

Similarly, we define

$$\rho_{M,N} = \frac{\delta_{M,N}^{(avg)}}{\delta_{1,1}^{(avg)}} \tag{34}$$

in order to evaluate the effect of adding in extra RRHs and TDs.

We plot $\xi_{M,N}$ and $\rho_{M,N}$ for multiple combinations of M and N in Fig. 21. It is observed that $\xi_{M,N}$ is above $\rho_{M,N}$ for each combination. Note that the achievable data rate of a TD is the product of the spectral efficiency and the bandwidth. We define the achievable downlink data rate of a single TD in the TR based C-RAN as $R_{M,N}^{TR} = r_{M,N}^{(avg)} \times W^{TR}$ where W^{TR} is the bandwidth that a TR based TD utilizes, and the achievable downlink data rate of a single TD in the LTE based C-RAN as $R_{M,N}^{LTE} = \delta_{M,N}^{(avg)} \times W^{LTE}$ where W^{LTE} is the bandwidth that a LTE based TD utilizes. In the TR based system, since larger bandwidth can be easily utilized with much reduced cost [21], the $R_{1,1}^{TR}$ can be greater than $R_{1,1}^{LTE}$ by utilizing larger bandwidth. For example, in this experiment, $W^{TR} = 125MHz$ and $W^{LTE} = 20MHz$. By $\xi_{M,N}$ and $\rho_{M,N}$ in Fig. 21 where $r_{M,N}^{(avg)}$ and $\delta_{M,N}^{(avg)}$ are normalized to $r_{1,1}^{(avg)}$ and $\delta_{1,1}^{(avg)}$, $R_{M,N}^{TR}$ will be greater than $R_{M,N}^{LTE}$ for any M and N. It means that the TR-based C-RAN is able to more efficiently utilize the wireless channel in the multiple-RRH and multiple-TD setting.

VI. Conclusion

In this work, we proposed a time-reversal (TR) based cloud radio access network (C-RAN) architecture. Both the downlink and uplink working schemes were designed and analyzed. Through analysis, we discovered the TR "tunneling" effect in the proposed C-RAN architecture, i.e., the baseband signals for multiple terminal devices (TDs) can be efficiently combined and transmitted in the front-haul link to alleviate the traffic load. We built a TR radio prototype to measure the wireless channel in the real-world environment, with which we illustrated the "tunneling" effect in both downlink and uplink of the proposed C-RAN architecture. It is observed that for both downlink and uplink, the sum spectral efficiency of multiple TDs increases with the number of TDs in the system while the front-haul data rate keeps almost constant. Based on the nice properties shown in this paper, the proposed TR-based C-RAN architecture serves as a promising solution to tackle the challenge to the C-RAN front-haul link capacity caused by network densification.

References

[1] Qualcomm, "1000x mobile data challenge," Tech. Rep., November 2013.

[2] ChinaMobile, "C-ran: The road towards green ran," *White Paper*, October 2011.

[3] M. Webb, Z. Li, P. Bucknell, T. Moulsley, and S. Vadgama, "Future evolution in wireless network architectures: Towards a 'cloud of antennas'," in *Vehicular Technology Conference (VTC Fall), 2012 IEEE*, Sept 2012, pp. 1–5.

[4] C.-L. I, J. Huang, R. Duan, C. Cui, J. Jiang, and L. Li, "Recent progress on c-ran centralization and cloudification," *IEEE Access*, vol. 2, pp. 1030–1039, 2014.

[5] Y. Beyene, R. Jantti, and K. Ruttik, "Cloud-ran architecture for indoor das," *IEEE Access*, vol. 2, pp. 1205–1212, 2014.

[6] A. Ghosh, R. Ratasuk, B. Mondal, N. Mangalvedhe, and T. Thomas, "Lte-advanced: next-generation wireless broadband technology [invited paper]," *IEEE Wireless Communications*, vol. 17, no. 3, pp. 10–22, June 2010.

[7] J. Lorca and L. Cucala, "Lossless compression technique for the fronthaul of lte/lte-advanced cloud-ran architectures," in *2013 IEEE 14th International Symposium and Workshops on a World of Wireless, Mobile and Multimedia Networks (WoWMoM)*, June 2013, pp. 1–9.

[8] R. Wang, H. Hu, and X. Yang, "Potentials and challenges of c-ran supporting multi-rats toward 5g mobile networks," *IEEE Access*, vol. 2, pp. 1187–1195, 2014.

[9] B. Dai and W. Yu, "Sparse beamforming and user-centric clustering for downlink cloud radio access network," *IEEE Access*, vol. 2, pp. 1326–1339, 2014.

[10] R. Zakhour and D. Gesbert, "Optimized data sharing in multicell mimo with finite backhaul capacity," *IEEE Transactions on Signal Processing*, vol. 59, no. 12, pp. 6102–6111, Dec 2011.

[11] Y. Zhou and W. Yu, "Optimized backhaul compression for uplink cloud radio access network," *IEEE Journal on Selected Areas in Communications*, vol. 32, no. 6, pp. 1295–1307, June 2014.

[12] X. Rao and V. Lau, "Distributed fronthaul compression and joint signal recovery in cloud-ran," *IEEE Transactions on Signal Processing*, vol. 63, no. 4, pp. 1056–1065, Feb 2015.

[13] S.-H. Park, O. Simeone, O. Sahin, and S. Shamai, "Inter-cluster design of precoding and fronthaul compression for cloud radio access networks," *IEEE Wireless Communications Letters*, vol. 3, no. 4, pp. 369–372, Aug 2014.

[14] O. Simeone, O. Somekh, H. V. Poor, and S. Shamai, "Downlink multicell processing with limited-backhaul capacity," *EURASIP Journal on Advances in Signal Processing*, vol. 2009, pp. 3:1–3:10, Feb. 2009.

[15] T. Strohmer, M. Emami, J. Hansen, G. Papanicolaou, and A. J. Paulraj, "Application of time-reversal with mmse equalizer to uwb communications," in *Global Telecommunications Conference, 2004. GLOBECOM'04. IEEE*, vol. 5. IEEE, 2004, pp. 3123–3127.

[16] C. Oestges, J. Hansen, S. M. Emami, A. D. Kim, G. Papanicolaou, and A. J. Paulraj, "Time reversal techniques for broadband wireless communication systems," in *European Microwave Conference (Workshop), Amsterdam, The Netherlands*, 2004, pp. 49–66.

[17] R. C. Qiu, C. Zhou, N. Guo, and J. Q. Zhang, "Time reversal with miso for ultrawideband communications: Experimental results," *IEEE Antennas and Wireless Propagation Letters*, vol. 5, no. 1, pp. 269–273, 2006.

[18] B. Wang, Y. Wu, F. Han, Y.-H. Yang, and K. J. R. Liu, "Green wireless communications: A time-reversal paradigm," *IEEE Journal on Selected Areas in Communications*, vol. 29, no. 8, pp. 1698–1710, September 2011.

[19] F. Han, Y.-H. Yang, B. Wang, Y. Wu, and K. J. R. Liu, "Time-reversal division multiple access over multi-path channels," *IEEE Transactions on Communications*, vol. 60, no. 7, pp. 1953–1965, July 2012.

[20] F. Han and K. J. R. Liu, "A multiuser trdma uplink system with 2d parallel interference cancellation," *IEEE Transactions on Communications*, vol. 62, no. 3, pp. 1011–1022, March 2014.

[21] Y. Chen, Y.-H. Yang, F. Han, and K. J. R. Liu, "Time-reversal wideband communications," *IEEE Signal Processing Letters*, vol. 20, no. 12, pp. 1219–1222, Dec 2013.

[22] H. Ma, F. Han, and K. J. R. Liu, "Interference-mitigating broadband secondary user downlink system: A time-reversal solution," in *Global Communications Conference (GLOBECOM), 2013 IEEE*, Dec 2013, pp. 884–889.

[23] Y. Chen, F. Han, Y.-H. Yang, H. Ma, Y. Han, C. Jiang, H.-Q. Lai, D. Claffey, Z. Safar, and K. J. R. Liu, "Time-reversal wireless paradigm for green internet of things: An overview," *IEEE Internet of Things Journal*, vol. 1, no. 1, pp. 81–98, Feb 2014.

[24] A. Goldsmith, *Wireless communications*. Cambridge university press, 2005.

[25] M. J. Golay, "Complementary series," *IRE Transactions on Information Theory*, vol. 7, no. 2, pp. 82–87, April 1961.

[26] Z.-H. Wu, Y. Han, Y. Chen, and K. J. Liu, "A time-reversal paradigm for indoor positioning system," *IEEE Transactions on Vehicular Technology*, vol. 64, no. 4, pp. 1331–1339, 2015.

[27] F. Weng, C. Yin, and T. Luo, "Channel estimation for the downlink of 3gpp-lte systems," in *2010 2nd IEEE International Conference on Network Infrastructure and Digital Content*, Sept 2010, pp. 1042–1046.

[28] B. Widrow and I. Kollár, *Quantization Noise: Roundoff Error in Digital Computation, Signal Processing, Control, and Communications*. Cambridge University Press, 2008.

[29] J. Gentle, *Computational Statistics*, ser. Statistics and Computing. Springer, 2009.

[30] J. Zyren and W. McCoy, "Overview of the 3gpp long term evolution physical layer," *Freescale Semiconductor Inc., white paper*, 2007.